Self-Propulsion of Pure Water Droplets by Spontaneous Marangoni-Stress-Driven Motion

Ziane Izri,[1] Marjolein N. van der Linden,[1] Sébastien Michelin,[2] and Olivier Dauchot[1,*]
[1]EC2M, UMR Gulliver 7083 CNRS, ESPCI ParisTech, PSL Research University, 10 rue Vauquelin, 75005 Paris, France
[2]LadHyX, Département de Mécanique, Ecole Polytechnique, CNRS, 91128 Palaiseau, France
(Received 23 June 2014; revised manuscript received 2 September 2014; published 11 December 2014)

We report spontaneous motion in a fully biocompatible system consisting of pure water droplets in an oil-surfactant medium of squalane and monoolein. Water from the droplet is solubilized by the reverse micellar solution, creating a concentration gradient of swollen reverse micelles around each droplet. The strong advection and weak diffusion conditions allow for the first experimental realization of spontaneous motion in a system of isotropic particles at sufficiently large Péclet number according to a straightforward generalization of a recently proposed mechanism [S. Michelin, E. Lauga, and D. Bartolo, Phys. Fluids 25, 061701 (2013); S. Michelin and E. Lauga, J. Fluid Mech. 747, 572 (2014)]. Experiments with a highly concentrated solution of salt instead of water, and tetradecane instead of squalane, confirm the above mechanism. The present swimming droplets are able to carry external bodies such as large colloids, salt crystals, and even cells.

DOI: 10.1103/PhysRevLett.113.248302 PACS numbers: 82.70.Kj, 47.63.mf, 47.20.Dr, 68.05.-n

The recent surge of interest in active systems has driven an intense research effort towards the design of self-propelled polar particles, including walking grains [1,2], rolling [3] or skating [4] colloids, and a variety of swimmers [5–9]. The latter often take the form of Janus-like colloids [10], named after the two-faced Roman god, because their motion originates from the asymmetry of their surface properties [7,8,11]. An alternative design of artificial swimmers consists of active droplets, either on interfaces [12,13] or in bulk fluid [14–17]. Droplets are particularly interesting systems since they are extensively used in microfluidic devices as (bio)chemical reactors [18,19]. Replacing the external flow transport of the droplets by self-propulsion would open new ways towards yet unexplored applications.

The self-propulsion mechanism of swimming droplets [14–17] has its origin in the Marangoni flow induced by a surface-tension gradient. In most cases, this gradient is maintained through specific chemical reactions, including the hydrolysis [14,15] or the bromination of the surfactant [16]. Liquid crystal droplets, stabilized by ionic surfactant, were also shown to develop spontaneous motion under certain circumstances of adsorption-depletion of the surfactant at the droplet interface [17]. Apart from being specific, these conditions may also be undesirable due to possible interactions between the chemicals and the products that are to be transported in the droplets.

Recently, it was shown theoretically that at sufficiently large Péclet number (strong advection, weak diffusion) the nonlinear interplay between surface osmotic flows and solute advection can produce spontaneous and self-sustained motion of isotropic particles [20,21]. In principle, sufficiently large droplets generating a solute of sufficiently large molecules or nanoparticles should thus self-propel without requiring any sort of chemical reaction.

In this Letter, we demonstrate experimentally the self-propulsion of pure water droplets in a biocompatible oil (squalane)–surfactant (monoolein) medium [Fig. 1(a)]. To the best of our knowledge, our system also constitutes the simplest realization of spontaneous motion in a system of isotropic particles as predicted in Refs. [20,21]. Replacing water with a saturated solution of salt, or squalane with tetradecane, we prove the robustness of the swimming mechanism. Finally, we take advantage of this robustness to illustrate the carrier function of these new swimming droplets, by transporting large colloids, salt crystals (which form in the saturated salt solution), and Dami cells [22] [Fig. 1(b)] inside the droplets.

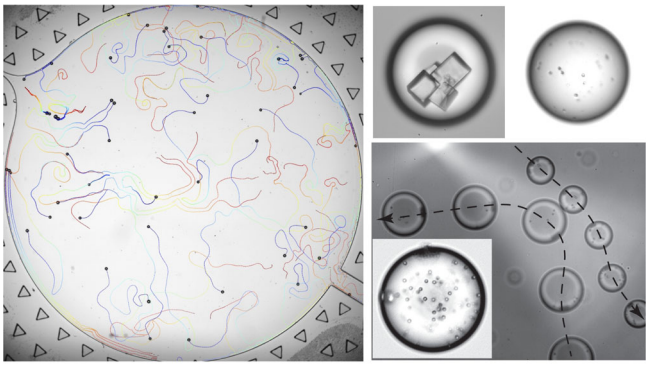

(a) (b)

FIG. 1 (color online). (a) Pure water droplet motion. Trajectories of ≃50 water droplets in the observation room (diameter 1 cm) filled with Sq–25 mM MO, recorded during 500 s. The droplet trajectory is color coded with the time preceding its present location (see movie in Supplemental Material [23]). (b) Swimming droplets as microfluidic carriers. Transport of salt crystals (top left), Dami cells [22] (top right), and colloids (bottom).

 © 2014 American Physical Society

The experimental system consists of pure water droplets (milli-Q) with typical radii a of 20–60 μm in a continuous oil-surfactant phase consisting of a solution of 25 mM of the nonionic surfactant monoolein (MO; 1-oleoyl-*rac*-glycerol, 99%, Sigma) in the oil squalane (Sq; 99%, Aldrich). The surfactant concentration is far above the critical micellar concentration (CMC) for MO in Sq (1.5 mM [16]). We also use droplets consisting of an almost saturated solution of 26 wt % NaCl (Sigma-Aldrich) in water and replace the continuous phase with tetradecane (Td; $\geq$ 99%, Aldrich) with 25 mM MO. The microfluidic device is made up of a 150-μm layer of UV-curing glue (Norland Optical Adhesive No. 81) on top of a cover slip held between two microscope slides [30]. The device comprises a T junction for droplet production with a channel section of 50×50 μm^2 and a circular observation chamber with a diameter of 1.0 cm and a height of 150 μm. Initially, the whole system is filled with the oil-surfactant solution. Water droplets are then produced at the T junction using typical flow rates of 10–50 μl/h and sent to a trash channel until the desired droplet size and density are obtained. We then redirect the flow towards the observation chamber and send 10–100 droplets into the chamber by greatly increasing the oil flow rate (to typically 1000 μl/h). When the droplets reach the center of the chamber we stop all flows. Images are recorded (Falcon II camera, Teledyne Dalsa) on a Nikon AZ100 macroscope (AZ Plan APO $1 \times$ NA 0.1 objective) for 2 h at $3 \times$ magnification and an acquisition rate of 1 frame per second. We obtain the droplet coordinates by processing the images in Labview using object and circle detection algorithms. Droplet trajectories are tracked using a Matlab algorithm adapted from Ref. [31].

First, we describe the droplet dynamics in the Sq-MO solution. After the fluid flows are stopped, the droplets move spontaneously in random directions. Figure 1(a) displays a picture of 50 droplets in the observation chamber, together with their trajectories recorded during a period of 500 s before the picture is taken. The droplets exhibit curved trajectories with a typical persistence length of the order of 500 μm. Interactions between the droplets are rather involved: we observe repulsion when the droplets move fast, but also attraction when they are slower. Some droplets form pairs and swim in parallel [see center of Fig. 1(a)]. In the following we concentrate on dilute systems and the short-time dynamics. The characterization of the long-time dynamics and possible collective effects are left for future work.

Typically, initial velocities are in the range 10–50 μm/s and the swimming motion lasts for 2 h, during which the velocity decays exponentially with time, with a characteristic decay time $\tau_v \simeq 3500$ s [Fig. 2(a)]. As a result the trajectory length extends up to several thousand droplet diameters, a "cruising range" never achieved before. A remarkable observation is that the droplet size also

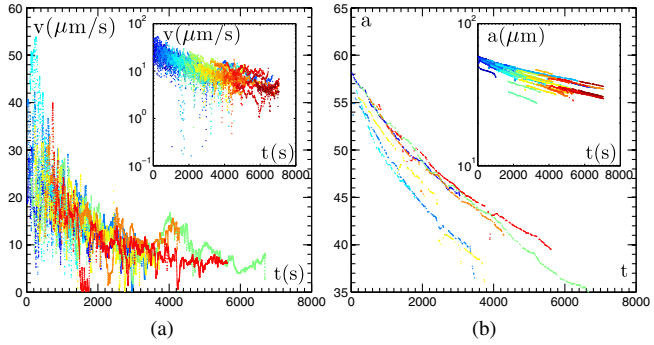

FIG. 2 (color online). Pure water droplet motion. (a) Velocity and (b) diameter versus time for a selection of eight trajectories. Insets: Linear-log plot for a selection of 35 trajectory parts.

decreases as a function of time [Fig. 2(b)]. The exponential decay is not as clear as for the velocity, but we can still estimate a characteristic decay time $\tau_a \simeq 8000$ s. From this very basic observation, we infer that there is, in one form or another, a net flux of water coming from the droplet at an almost constant rate $\kappa = a(0)/\tau_a \simeq 5 \times 10^{-3}$ μm s^{-1}, where $a(0)$ is the initial droplet radius. A natural question is how the velocity scales with the droplet radius. However, as can readily be seen in Fig. 2(a), there are very strong fluctuations of the velocity: a droplet may slow down by more than a factor of 100 before recovering its nominal velocity.

Such fluctuations are completely absent from the radius dynamics [Fig. 2(b)], suggesting the existence of at least one other parameter controlling the instantaneous droplet velocity. Figure 3(a) represents a typical trajectory, which has been colored according to the instantaneous tangential acceleration of the droplet. Straight parts of the trajectories have small tangential acceleration, while curved parts of the trajectory are preceded by a negative acceleration and followed by a positive one. This is confirmed in Fig. 3(b), where the instantaneous velocity v is plotted as a function of the instantaneous radius of curvature R (the time is color coded from blue to red). Each time the radius of curvature decreases below, say, 500 μm, the velocity decreases strongly and subsequently increases again with increasing radius of curvature. For a radius of curvature larger than 500 μm, the velocity depends only on time. We checked that after filtering the velocity data and retaining only the parts of the trajectories with $R > 500$ μm, the fluctuations observed in Fig. 2(a) are suppressed. Note that, in the absence of inertia, one should not interpret these observations in terms of "cautious driving." Here, the curvature presumably results from the repulsion between the droplets, which in addition slows the droplets down when they approach and speeds them up when they separate.

Before discussing the mechanism of self-propulsion, we consider the robustness of the phenomena. Table I lists the various systems we have examined. We have separately varied the surfactant, the oil, and the composition inside

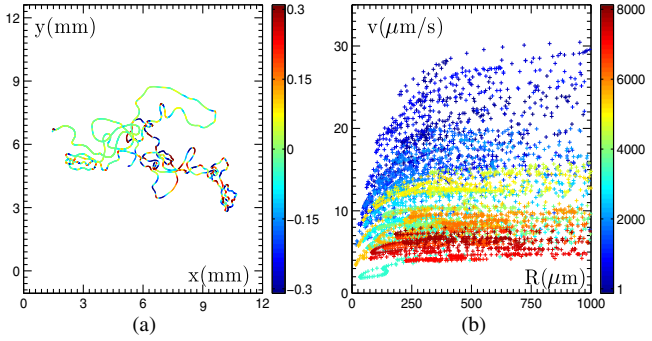

FIG. 3 (color online). Correlation between velocity and local radius of curvature of the trajectory. (a) A typical trajectory colored by the instantaneous tangential acceleration ($\mu m\,s^{-2}$). (b) Velocity as a function of the radius of curvature of the trajectory shown in (a). The color code indicates time (s) from the beginning of the trajectory.

the droplet. The present list is by no means exhaustive, but aims at testing basic variations in search of the essential ingredients of the underlying swimming mechanism. The first result is that MO as a surfactant is a key ingredient of the microscopic mechanism responsible for swimming. Neither Span 80 nor oleic acid, which have the same apolar tail but different polar head groups, leads to swimming motion [32]. Furthermore, it is crucial that the MO concentration is above the CMC, telling us that micelles play a key role in the physicochemical mechanism. When Sq is replaced with Td, the swimming motion still occurs, suggesting that the choice of the continuous phase is not as crucial. However, the use of water-saturated Sq, obtained by keeping the Sq-MO system in contact with water during several days, suppresses the swimming motion. This clearly indicates that gradients of water (in some form) around the droplet are essential to the swimming mechanism. Coming now to the discrete phase, we added NaCl to the water in order to test whether osmotic pressure, which tends to keep water inside the droplet, would prevent swimming. As we show below, the presence of salt alters the swimming motion, but does not suppress it, even at a salt concentration of 26 wt %, close to saturation. Finally, inspired by the work of Thutupalli *et al.* on swimming water droplets [16], we added successively all the compounds of the Belousov-Zhabotinski (BZ) reaction (sulfuric acid, sodium bromate, malonic acid) to the water, *except* for the catalyst, using the same concentrations as in Ref. [16]. Amazingly, the droplets are still swimming, suggesting that the mechanism at play in the present work may also be present in the system of Ref. [16]. Focusing more quantitatively on the most relevant systems described above, namely, the water in Sq-MO, the water in Td-MO, and the salt-saturated water in Sq-MO systems, it is observed [see Fig. 4(a) and Table II] that a larger decay rate of the droplet size $\langle\kappa\rangle$ corresponds to a faster initial swimming velocity $\langle v(0)\rangle$ and a shorter duration of the swimming motion $T_{\rm swim}$.

TABLE I. Realization of swimming motion for various water-oil-surfactant systems. The surfactant concentration is above the CMC unless indicated otherwise (see text for details).

Discrete phase	Continuous phase	Surfactant	Motion
H_2O	Sq	MO	Yes
H_2O	Sq	MO (< CMC)	No
H_2O	Sq	Span 80	No
H_2O	Sq	Oleic acid	No
H_2O	Td	MO	Yes
H_2O	Water-saturated Sq	MO	No
H_2O + salt	Sq	MO	Yes
H_2O + malonic acid	Sq	MO	Yes
H_2O + inhibited BZ	Sq	MO	Yes

From the macroscopic observations (the droplet radius decreases in time) we know that, in some form or another, water leaves the droplets, hence producing a gradient of solute outside each droplet. This is a situation very similar to the one investigated theoretically in Refs. [20,21]: a spherical particle of radius a emits ($A > 0$) or captures ($A < 0$) a solute with a uniform surface emission rate (activity) A. The solute interacts with the spherical particle on a small length scale $\lambda \ll a$, giving rise, whenever a surface gradient of solute $\nabla_\parallel C$ develops, to a slip velocity $v^s = M\nabla_\parallel C$ that drives a net flow outside the particle. The phoretic mobility $M \approx \pm k_B T\lambda^2/2\eta_o$, where η_o is the viscosity of the surrounding fluid, can be either positive or negative depending on the particle surface-solute interaction potential [33]. The trivial solution to the coupled Stokes flow and advection-diffusion of the solute corresponds to an isotropic solute concentration and no fluid motion. However, when $AM > 0$, this isotropic solution is linearly unstable above a critical Péclet number

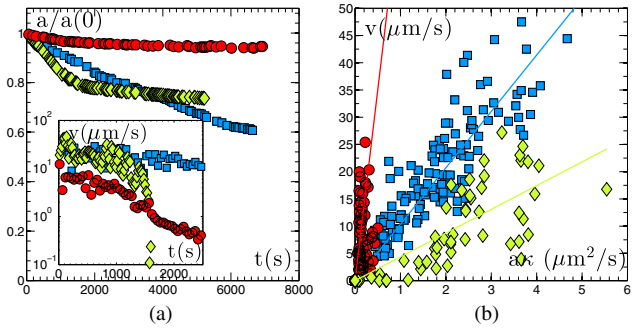

FIG. 4 (color online). Comparison of three different systems. (a) Decay of the relative droplet radius versus time for three droplets under different conditions: water in Sq-MO (blue squares), water in Td-MO (green diamonds), water-26 wt % NaCl in Sq-MO (red circles). Inset: Velocity versus time for the same three droplets. (b) Parametric plot of the velocity versus $a \times \kappa$ for droplets under the same three different sets of conditions; each point represents a different droplet during a different period of time corresponding to a straight part of its trajectory.

TABLE II. Swimming motion characteristics at initial times for three systems of interest: (1) H_2O in Sq-MO, (2) H_2O in Td-MO, (3) $H_2O + 26$ wt % NaCl (see text for details).

System	$\langle D(0)\rangle$	$\langle \kappa(0)\rangle$ (μm/s)	$\langle v(0)\rangle$ (μm/s)	T_{swim} (h)
(1)	91 ± 5	$4.5 \times 10^{-2} \pm 5 \times 10^{-3}$	20 ± 2	2
(2)	93 ± 5	$7.5 \times 10^{-2} \pm 5 \times 10^{-3}$	22 ± 2	1/2
(3)	63 ± 5	$1.2 \times 10^{-2} \pm 5 \times 10^{-3}$	11 ± 2	> 2

$\text{Pe} = U^* a/D$, where $U^* = |AM|/D$ is the characteristic autophoretic velocity and D is the diffusion coefficient of the solute. This leads to a spontaneous symmetry breaking of the concentration field and propulsion (see Fig. 5, with $\eta_i \to \infty$).

Extending this result to active droplets follows easily from two essential properties shared with the autophoretic particle problem: (i) the solute is released at the droplet's surface and advected by the outer flow and (ii) this flow results from tangential motion of the surface of an impermeable force-free spherical body. The two configurations differ, however, on the existence of a flow within the droplet with viscosity η_i, and on the hydrodynamic boundary conditions at the interface: the slip velocity is replaced by an analogous velocity jump $v^j = M\nabla_\parallel C$ (phoretic effect) complemented by a tangential stress jump $\tau^j = -\nabla_\parallel \gamma$ across the interface (Marangoni effect). The surface tension gradient originates from a number of physicochemical mechanisms, including the solute-surface interaction or potentially the desorption of the surfactant from the interface [17]. The common cause for all these mechanisms is $\nabla_\parallel C$, and to linear order, we expect $\nabla_\parallel \gamma = K\nabla_\parallel C$, where $K \approx \pm k_B T\lambda$. Under this assumption, the droplet velocity is now obtained as [33]

$$\mathbf{U} = -M'\langle \nabla_\parallel C\rangle, \quad \text{with} \quad M' \equiv \frac{aK + 3\eta_i M}{2\eta_o + 3\eta_i}, \qquad (1)$$

where $\langle\cdot\rangle$ denotes the average over the interface.

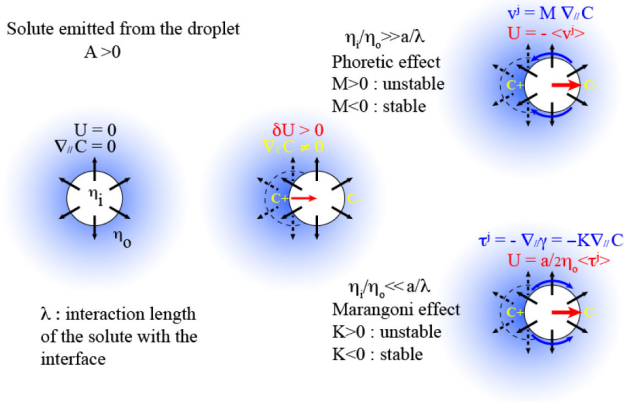

FIG. 5 (color online). Swimming mechanism behind the spontaneous autophoretic and Marangoni-driven motions of an isotropic droplet.

Repeating the analysis of Ref. [20], we consider an axisymmetric perturbation of the isotropic concentration distribution $\bar{C}(r) = Aa^2/Dr$. Its first azimuthal moment, $C_1'(r,t)$, satisfies at leading order

$$\frac{\partial C_1'}{\partial t} - \frac{D}{r^2}\left[\frac{\partial}{\partial r}\left(r^2\frac{\partial C_1'}{\partial r}\right) - 2C_1'\right] = \frac{Aa^2U}{Dr^2}\left(\frac{a^3}{r^3} - 1\right). \qquad (2)$$

Because $\langle \nabla_\parallel C\rangle = 2C_1'(a,t)\mathbf{e}_z/3a$, Eqs. (1) and (2) are strictly identical to the dimensional form of Eqs. (10) and (11) of Ref. [20]. The linear stability results are therefore directly applicable here provided the phoretic mobility M is replaced by M'. The change in boundary conditions impacts, however, the nonlinear dynamics and steady-state velocity (see Supplemental Material [23]).

The relative importance of Marangoni and phoretic effects is given by the comparison of the viscosity ratio η_i/η_o with the length scale ratio a/λ. For droplets in general, and in the present case in particular ($\eta_i/\eta_o = 1/36$), Marangoni effects largely dominate so that $M' = (aK/2\eta_o)$. The spontaneous propulsion of the droplets indicates that the delicate balance of the physicochemical mechanisms at play ensures $K > 0$, the necessary condition for the linear instability to take place, provided the Péclet number $\text{Pe} = (AM'a/D^2)$ is greater than $\text{Pe}_c = 4$ [20].

In order to proceed, we specify in what form water leaves the droplets. We have seen that empty reverse micelles of MO are necessary for the realization of the swimming motion. Following Refs. [17,34], we propose that the water is solubilized by the reverse micelles that are present in the continuous oil phase, forming swollen reverse micelles that act as the "solute." This is consistent with the observation that using a water-saturated Sq-MO oil phase prevents both the shrinkage and the swimming of the droplets. Furthermore, dynamic light scattering experiments on the Td-MO oil phase that had been in contact with water droplets for 1–3 h, which were removed by centrifugation, reveal a typical radius $\delta \approx 10$ nm for the swollen reverse micelles, while no objects of this size are present in the native oil phase.

In the present context, the activity A is easily related to the decrease rate of the droplet radius $\kappa = |da/dt|$ by equating the number of swollen reverse micelles of radius δ formed per unit time, $dN/dt = 4\pi a^2 A$, to the change in volume of the droplet divided by the volume of a swollen reverse micelle, $(1/\delta^3)(da^3/dt) = 3\kappa(a^2/\delta^3)$, from which

it follows that $A = (3/4\pi)(\kappa/\delta^3)$. Taking the diffusion coefficient of the solute $D = k_B T/(6\pi\eta_o\delta)$, we then obtain for the typical droplet velocity

$$U^* = \frac{AM'}{D} \approx \frac{9}{4}\kappa\frac{a\lambda}{\delta^2}. \quad (3)$$

The linear scaling of the droplet velocity with κa is indeed observed in Fig. 4(b). Furthermore, assuming $\lambda \simeq \delta$ and $\delta \approx 10$ nm, we find a characteristic velocity of a few tens of μm/s and Pe $\gg 1$, in agreement with the observations and the linear instability condition.

In summary, we have established the first experimental evidence of spontaneous swimming of pure water droplets. The conditions of swimming are threefold: (i) water droplets must be stabilized in an oil medium with surfactant above CMC; (ii) the surfactant inverse micelles must be prone to extract water from the droplets; (iii) the Péclet number must be large enough (large droplets, high oil viscosity, fast kinetics of the water transfer to the micelles). Apart from confirming a very general instability mechanism, it opens new ways to a plethora of applications. As a first step in this direction, we have demonstrated the versatility of these droplets as universal carriers: Figure 1(b) illustrates the transport of colloids, salt crystals, and cells. We found that the swimming of the droplets was also maintained for pH $\in$ (3–11). Such robustness indicates that there is room for optimization, which in turn calls for a detailed investigation of the physicochemical mechanisms at play.

The authors thank Denis Bartolo for his help with microfluidics and enlightening discussions, the MMN lab for their help in designing microfluidic devices, Bérengère Abou for her support in performing the DLS measurements, and Antoine Blin for providing the cells. The project was supported by Agence Nationale de la Recherche, Microfluidic Traffic, and M. N. v. d. L. was sponsored by a postdoctoral fellowship from Domaine d'Intérêt Majeur, Institut des Systèmes Complexes.

Z. I. and M. N. v. d. L. contributed equally to this work.

*olivier.dauchot@espci.fr

[1] J. Deseigne, S. Léonard, O. Dauchot, and H. Chaté, Soft Matter **8**, 5629 (2012).
[2] J. Deseigne, O. Dauchot, and H. Chaté, Phys. Rev. Lett. **105**, 098001 (2010).
[3] A. Bricard, J.-B. Caussin, N. Desreumaux, O. Dauchot, and D. Bartolo, Nature (London) **503**, 95 (2013).
[4] J. Palacci, S. Sacanna, A. P. Steinberg, D. J. Pine, and P. Chaikin, Science **339**, 936 (2013).
[5] W. F. Paxton, S. Sundararajan, T. E. Mallouk, and A. Sen, Angew. Chem., Int. Ed. Engl. **45**, 5420 (2006).
[6] P. Poesio, G. P. Beretta, and T. Thorsen, Phys. Rev. Lett. **103**, 064501 (2009).
[7] J. Palacci, C. Cottin-Bizonne, C. Ybert, and L. Bocquet, Phys. Rev. Lett. **105**, 088304 (2010).
[8] I. Theurkauff, C. Cottin-Bizonne, J. Palacci, C. Ybert, and L. Bocquet, Phys. Rev. Lett. **108**, 268303 (2012).
[9] W. Poon, *Proceedings of the International School of Physics "Enrico Fermi", Course CLXXXIV "Physics of Complex Colloids"*, edited by C. Bechinger, F. Sciortino, and P. Ziherl (IOS, Amsterdam: SIF, Bologna, 2013), Vol. 184, p. 317.
[10] A. Walther and A. H. E. Müller, Soft Matter **4**, 663 (2008).
[11] J. R. Howse, R. Jones, A. Ryan, T. Gough, R. Vafabakhsh, and R. Golestanian, Phys. Rev. Lett. **99**, 048102 (2007).
[12] Y.-J. Chen, Y. Nagamine, and K. Yoshikawa, Phys. Rev. E **80**, 016303 (2009).
[13] S. Yabunaka, T. Ohta, and N. Yoshinaga, J. Chem. Phys. **136**, 074904 (2012).
[14] T. Toyota, N. Maru, M. M. Hanczyc, T. Ikegami, and T. Sugawara, J. Am. Chem. Soc. **131**, 5012 (2009).
[15] M. M. Hanczyc, T. Toyota, T. Ikegami, N. Packard, and T. Sugawara, J. Am. Chem. Soc. **129**, 9386 (2007).
[16] S. Thutupalli, R. Seemann, and S. Herminghaus, New J. Phys. **13**, 073021 (2011).
[17] S. Herminghaus, C. C. Maass, C. Krüger, S. Thutupalli, L. Goehring, and C. Bahr, Soft Matter **10**, 7008 (2014).
[18] A. J. deMello, Nature (London) **442**, 394 (2006).
[19] L. Baraban, F. Bertholle, M. L. M. Salverda, N. Bremond, P. Panizza, J. Baudry, J. A. G. M. de Visser, and J. Bibette, Lab Chip **11**, 4057 (2011).
[20] S. Michelin, E. Lauga, and D. Bartolo, Phys. Fluids **25**, 061701 (2013).
[21] S. Michelin and E. Lauga, J. Fluid Mech. **747**, 572 (2014).
[22] S. M. Greenberg, D. S. Rosenthal, T. A. Greeley, R. Tantravahi, and R. I. Handin, Blood **72**, 1968 (1988).
[23] See Supplemental Material at http://link.aps.org/supplemental/10.1103/PhysRevLett.113.248302, which includes Refs. [24–29], for a detailed description of the coupled Stokes and advection-diffusion problem and a movie corresponding to Fig. 1(a) (100x faster than real time).
[24] J. R. Blake, J. Fluid Mech. **46**, 199 (1971).
[25] J. Happel and H. Brenner, *Low Reynolds Number Hydrodynamics* (Prentice-Hall, Englewood Cliffs, NJ, 1965).
[26] E. Lauga and T. R. Powers, Rep. Prog. Phys. **72**, 096601 (2009).
[27] L. G. Leal, *Advanced Transport Phenomena, Fluid Mechanics and Convective Transport Processes* (Cambridge University Press, New York, 2007).
[28] S. Michelin and E. Lauga, Phys. Fluids **23**, 101901 (2011).
[29] S. Michelin and E. Lauga, J. Fluid Mech. **715**, 1 (2013).
[30] D. Bartolo, G. Degré, P. Nghe, and V. Studer, Lab Chip **8**, 274 (2008).
[31] J. C. Crocker and D. G. Grier, J. Colloid Interface Sci. **179**, 298 (1996).
[32] The polar head group affects the packing parameter of the surfactant and thus the tendency of the reverse micelles to solubilize water from the droplet. At first sight, we expect the packing parameter to decrease in the order of increasing hydrophilic-lipophilic balance (HLB) value: oleic acid (HLB = 1), monoolein (HLB = 3.8), Span 80 (HLB = 4.3). However, this does not explain why only monoolein leads to swimming motion.
[33] J. L. Anderson, Annu. Rev. Fluid Mech. **21**, 61 (1989).
[34] K. Shinoda and T. Ogawa, J. Colloid Interface Sci. **24**, 56 (1967).

Supplemental material for "Self-propulsion of pure water droplets by spontaneous Marangoni stress driven motion"

Ziane Izri,[1] Marjolein N. van der Linden,[1] Sébastien Michelin,[2] and Olivier Dauchot[1]

[1]*EC2M, UMR Gulliver 7083 CNRS, ESPCI ParisTech, PSL Research University, 10 rue Vauquelin, 75005 Paris, France*

[2]*LadHyX – Département de Mécanique, Ecole Polytechnique – CNRS, 91128 Palaiseau, France*

In the main manuscript, we showed that the linear stability analysis for an isotropic active droplet is essentially identical to that of an active autophoretic particle provided the phoretic mobility M is replaced by

$$M' = \frac{aK + 3\eta_i M}{2\eta_o + 3\eta_i}, \tag{1}$$

where η_i and η_o are the fluid viscosities inside and outside the droplet, respectively, and K defines the linear relationship between the local surface tension gradient $\nabla_\parallel \gamma$ and the local solute concentration gradient. In this supplementary material, we provide the full details on the coupled Stokes and advection-diffusion problem, and show that although qualitatively similar the nonlinear dynamics and saturation velocity differ between the droplet and solid particle cases.

The droplet is assumed to remain spherical at all times (i.e. the capillary number $\mathrm{Ca} = \eta U^*/\gamma$ is small where U^* is the characteristic droplet velocity). The normal unit vector at the surface is $\mathbf{n} = \mathbf{e}_r$, and $\nabla_\parallel = (\mathbf{I} - \mathbf{nn}) \cdot \nabla$ is the tangential gradient operator. We focus on an axisymmetric problem such that all fields depend only on r and $\mu = \cos\theta$, with θ the polar angle in spherical polar coordinates.

The solute is released from the droplet's surface ($r = a$) at a constant flux A, such that the boundary condition for the solute dynamics on the droplet's surface can be written as

$$D\mathbf{n} \cdot \nabla C|_{(r=a)} = -A. \tag{2}$$

The solute is then advected by the outer flow and diffuses with diffusivity D:

$$\frac{\partial C}{\partial t} + \mathbf{u}^o \cdot \nabla C = D\nabla^2 C. \tag{3}$$

A uniform concentration C_∞ is assumed in the far-field (e.g. zero). Flows inside and outside the droplet satisfy Stokes equations (i.e. the Reynolds number $\mathrm{Re} = U^* a/\eta$ is small)

$$\eta_i \nabla^2 \mathbf{u}^{o,i} = \nabla p^{o,i}, \quad \nabla \cdot \mathbf{u}^{o,i} = 0, \tag{4}$$

where superscripts ^{i} and ^{o} on hydrodynamic fields refer to the inner ($r < a$) and outer ($r > a$) flows, respectively. Considering a reference frame attached to the droplet's center, the boundary condition at infinity is obtained as

$$\mathbf{u}^o(r \to \infty) \sim -\mathbf{U}, \tag{5}$$

with $\mathbf{U}$ the droplet's velocity (there is no rotation here due to the axisymmetry). At the droplet's surface, inhomogeneities in the local solute concentration lead to tangential velocity and stress jumps:

$$\mathbf{u}_j = \left(\mathbf{u}^o - \mathbf{u}^i\right)_{(r=a)} = M\, \nabla_\parallel C\big|_{(r=a)}\,, \tag{6}$$

$$\boldsymbol{\tau}_j = \left[(\mathbf{I} - \mathbf{nn}) \cdot \left(\boldsymbol{\sigma}^o - \boldsymbol{\sigma}^i\right) \cdot \mathbf{n}\right]_{(r=a)} = \nabla_\parallel \gamma\big|_{(r=a)} = -\,K \nabla_\parallel C\big|_{(r=a)}\,. \tag{7}$$

Finally, inertia is negligible and assuming there is no external body force (e.g. buoyancy), the droplet must remain force-free at all times

$$\int_{(r=a)} \boldsymbol{\sigma}^o \cdot \mathbf{n} \mathrm{d}S = 0. \tag{8}$$

Equations (2)–(8) form a closed and well-posed set of equations for the solute concentration $C(r, \mu)$ outside the droplet and the flow fields $\mathbf{u}^i$ and $\mathbf{u}^o$ inside and outside the droplet. Because of the spherical geometry, the hydrodynamic problem, Eqs. (4)–(5) and (8) can be solved formally and analytically as follows, using the squirmer model [1, 5]. The flow is axisymmetric, and can therefore be computed from the streamfunction $\psi(r, \mu, t)$, as

$$\mathbf{u} = -\frac{1}{r^2}\frac{\partial \psi}{\partial \mu}\mathbf{e}_r - \frac{1}{r\sqrt{1-\mu^2}}\frac{\partial \psi}{\partial r}\mathbf{e}_\theta. \tag{9}$$

The streamfunction $\psi(r,\mu,t)$ is decomposed azimuthally inside and outside the droplet,

$$\psi^{o,i}(r,\mu,t) = \sum_{n=1}^{\infty} \frac{2n+1}{n(n+1)} \alpha_n^{o,i}(t) \psi_n^{o,i}(r)(1-\mu^2)L_n'(\mu), \tag{10}$$

with $L_n(\mu)$ the Legendre polynomial of order n. $\alpha_n^o(t)$ and $\alpha_n^i(t)$ are the outer and inner squirming mode intensities and may differ when the velocity jump $\mathbf{u}_j$ is non zero. Inside and outside the droplet, the radial part of the streamfunction must be of the form [2, 4]

$$\psi_n^{o,i}(r) = E_n^{o,i} r^{n+3} + F_n^{o,i} r^{n+1} + G_n^{o,i} r^{2-n} + H_n^{o,i} r^{-n}, \tag{11}$$

where $E_n^{o,i}, F_n^{o,i}, G_n^{o,i}$ and $H_n^{o,i}$ are constants to be determined using regularity and boundary conditions in each domain. Using the force-free condition, Eq. (8) ($G_1^o = 0$), the impermeability condition ($\psi_n^o(a) = 0$) and the far-field behavior of the flow, Eq. (5), the outer radial modes $\psi_n^0(r)$ are obtained as [4, 5]

$$\psi_1^o(r) = \frac{a^3}{3r} - \frac{r^2}{3}, \qquad \psi_n^o(r) = \frac{1}{2}\left(\frac{a^{n+2}}{r^n} - \frac{a^n}{r^{n-2}}\right) \quad \text{for } n \geq 2. \tag{12}$$

In particular, $\alpha_1^o(t) = U(t)$ is the swimming velocity of the droplet. The second mode, $n = 2$, corresponds to the intensity of the slowest-decaying singularity created by the self-propelled droplet, namely that of a symmetric force dipole or stresslet. Enforcing the regularity of the flow field inside the droplet ($G_n^i = H_n^i = 0$) and the impermeability condition ($\psi_n^i(a) = 0$), the inner radial modes $\psi_n^i(r)$ are obtained as

$$\psi_n^i(r) = \frac{1}{2}\left(\frac{r^{n+1}}{a^{n-1}} - \frac{r^{n+3}}{a^{n+1}}\right). \tag{13}$$

Finally, decomposing the solute concentration azimuthally, $C(r,\mu,t) = \sum C_p(r,t)L_p(\mu)$, the different modes $C_p(r,t)$ satisfy the following system of partial differential equations in the outer fluid:

$$\frac{\partial C_p}{\partial t} + \frac{1}{r^2}\sum_{m=0}^{\infty}\sum_{n=1}^{\infty} \alpha_n^o(t)\left(A_{mnp}\frac{\partial C_m}{\partial r}\psi_n^o + B_{mnp}C_m\frac{\mathrm{d}\psi_n^o}{\mathrm{d}r}\right) = \frac{D}{r^2}\left[\frac{\partial}{\partial r}\left(r^2\frac{\partial C_p}{\partial r}\right) - p(p+1)C_p\right], \tag{14}$$

with boundary conditions

$$D\frac{\partial C_p}{\partial r}(r=a) = -A\delta_{p0}, \qquad C_p(r\to\infty) \to C_\infty\delta_{p0}. \tag{15}$$

The tensors A_{mnp} and B_{mnp} are defined as

$$A_{mnp} = \frac{(2p+1)(2n+1)}{2}\int_{-1}^{1} L_m(\mu)L_n(\mu)L_p(\mu)\mathrm{d}mu, \quad B_{mnp} = \frac{(2p+1)(2n+1)}{2n(n+1)}\int_{-1}^{1}(1-\mu^2)L_m'(\mu)L_n'(\mu)L_p(\mu)\mathrm{d}\mu \tag{16}$$

The solute is released from the droplet's surface into the outer fluid only, where it is advected and diffuses. Hence, its dynamics is not impacted by the flow inside the droplet, and to solve this advection-diffusion problem for $C_p(r,t)$, one only needs to know the outside flow (i.e. $\alpha_n^o(t)$).

Using Eqs. (9) and (10), the velocity jump condition, Eq. (6), can now be written in terms of $\alpha_n^{o,i}$:

$$\alpha_n^o - \alpha_n^i = -\frac{n(n+1)}{2n+1}\frac{M}{a}C_n(a,t). \tag{17}$$

The stress jump condition, Eq. (7), writes

$$\left(\sigma_{r\theta}^o - \sigma_{r\theta}^i\right)(r=a) = \frac{K\sqrt{1-\mu^2}}{a}\frac{\partial C}{\partial \mu}(r=a) \tag{18}$$

with the stress tensor component $\sigma_{r\theta}$ obtained inside and outside the droplet using

$$\sigma_{r\theta}^{o,i} = \eta_{o,i}\left[r\frac{\partial}{\partial r}\left(\frac{u_\theta^{o,i}}{r}\right) - \frac{\sqrt{1-\mu^2}}{r}\frac{\partial u_r^{o,i}}{\partial \mu}\right] = -\eta_{o,i}\sqrt{1-\mu^2}\sum_{n=1}^{\infty}\frac{2n+1}{n(n+1)}\alpha_n^{o,i}(t)L_n'(\mu)\left[r\frac{\mathrm{d}}{\mathrm{d}r}\left(\frac{1}{r^2}\frac{\mathrm{d}\psi_n^{o,i}}{\mathrm{d}r}\right) + \frac{n(n+1)}{r^3}\psi_n^{o,i}\right]. \tag{19}$$

Applying the stress jump condition on $r = a$, we obtain

$$3\eta_o\alpha_1^o + \frac{9\eta_i}{2}\alpha_1^i = -KC_1(a,t), \qquad \eta_o\alpha_n^o + \eta_i\alpha_n^i = -\frac{n(n+1)}{(2n+1)^2}KC_n(a,t) \text{ for } n \geq 2. \tag{20}$$

Equations (17) and (20) form a linear system for α_n^o and α_n^i that can be inverted to obtain $\alpha_n^o(t)$ as a function of $C_n(a,t)$, and the entire flow field outside the droplet (the flow inside the droplet can be recovered similarly):

$$\alpha_1^o(t) = -\frac{2}{3}\left(\frac{aK + 3\eta_i M}{2\eta_o + 3\eta_i}\right)\frac{C_1(a,t)}{a}, \tag{21}$$

$$\alpha_n^o(t) = -\frac{n(n+1)}{(2n+1)^2}\left(\frac{aK + M\eta_i(2n+1)}{\eta_o + \eta_i}\right)\frac{C_n(a,t)}{a}, \tag{22}$$

As we pointed out earlier, the solute dynamics only requires the knowledge of the outer flow or $\alpha_n^o(t)$, as for the problem of a rigid phoretic particle. In both cases, $\alpha_n^o(t)$ is proportional to $C_n(a,t)$, Eqs. (21)–(22), but the coefficient of proportionality (and its variation with n) differs between the two cases.

Repeating the analysis of [8] in the case of a droplet, we consider the stability of the trivial isotropic and steady solution to the coupled Stokes and advection-diffusion problems above, $\bar{C}(r) = Aa^2/Dr$, which leads to no tangential gradients and therefore no flow ($\bar{\alpha}_n^{o,i} = 0$). Decomposing the perturbation $C'(r,\mu,t)$ azimuthally, the equation for the first azimuthal mode $C_1'(r,t)$ is obtained, at leading order in the perturbation, from Eq. (14) with $p = 1$ as

$$\frac{\partial C_1}{\partial t} - \frac{D}{r^2}\left[\frac{\partial}{\partial r}\left(r^2\frac{\partial C_1}{\partial r}\right) - 2C_1\right] = -\frac{3\alpha_1^o(t)}{r^2}\frac{\mathrm{d}\bar{C}}{\mathrm{d}r}\psi_1^o = \frac{\alpha_1^o(t)Aa^2}{Dr^2}\left(\frac{a^3}{r^3} - 1\right) \tag{23}$$

and one can observe that $\alpha_1^o(t)$ is the only squirming mode influencing the linear instability leading to self-propulsion. Hence, Eqs. (21) and (23) are strictly identical to the case of a rigid phoretic particle (Eqs. (10) and (11) in [8]) provided the substitution Eq. (1) is performed. The linear stability result of [8] for the swimming mode is therefore directly applicable to the droplet case and spontaneous self-propulsion of isotropic spherical droplets is predicted provided $AM' > 0$ and $\mathrm{Pe} = |AM'|a/D^2 \geq 4$. To investigate the nonlinear saturated dynamics beyond the instability threshold, all modes must be considered and the result is now modified from the rigid particle case.

In terms of swimming velocity, the rigid particle limit is recovered when $\eta_i M/aK \gg 1$ or equivalently given the scalings of M and K in the main text when $\eta_i/\eta_o \gg a/\lambda$ which is essentially only achieved for a rigid particle, since $\lambda \ll a$. For a droplet, the Marangoni terms dominate systematically, except for very high order modes as suggested by Eq. (22). From a numerical point of view however, in the Marangoni limit ($\eta_i/\eta_o \to \infty$), the convergence of the result with the number of squirming modes is faster than for the phoretic case ($\alpha_n^o = O(C_n)$ in the Marangoni limit rather than $\alpha_n^o = O(nC_n)$ in the phoretic limit). High-order modes therefore only have a negligible contribution to the flow field, except if $\mathrm{Pe} \gg 1$ (in that case the flow field and the solute distribution become strongly polarized azimuthally [6, 7]).

Equations (14), (15), (21) and (22) can be solved numerically using the numerical methods described in [6, 7] and the result is shown in Figure 1 in the pure Marangoni limit and with $\eta_i/\eta_o = 1/36$. The evolution of the velocity with Pe is qualitatively similar to that obtained by [8] for a rigid phoretic particle, albeit slightly larger. Also, as for rigid phoretic particles, self-propelling droplets are always pushers ($\Sigma < 0$), meaning that their far-field signature is similar to the flow field generated by flagellated bacteria [3].

[1] J. R. Blake. A spherical envelope approach to ciliary propulsion. *J. Fluid Mech.*, 46:199–208, 1971.

[2] J. Happel and H. Brenner. *Low Reynolds Number Hydrodynamics.* Prentice Hall, Englewood Cliffs, NJ, 1965.

[3] E. Lauga and T. R. Powers. The hydrodynamics of swimming micro-organisms. *Rep. Prog. Phys.*, 72:096601, 2009.

[4] L. G. Leal. *Advanced Transport Phenomena, Fluid Mechanics and Convective Transport Processes.* Cambridge University Press, New York, 2007.

[5] S. Michelin and E. Lauga. Optimal feeding is optimal swimming for all Péclet numbers. *Phys. Fluids*, 23(10):101901, 2011.

[6] S. Michelin and E. Lauga. Unsteady feeding and optimal strokes of model ciliates. *J. Fluid Mech.*, 715:1–31, 2013.

[7] S. Michelin and E. Lauga. Phoretic self-propulsion at finite péclet numbers. *J. Fluid Mech.*, 747:572–604, 2014.

[8] S. Michelin, E. Lauga, and D. Bartolo. Spontaneous autophoretic motion of isotropic particles. *Phys. Fluids*, 25:061701, 2013.

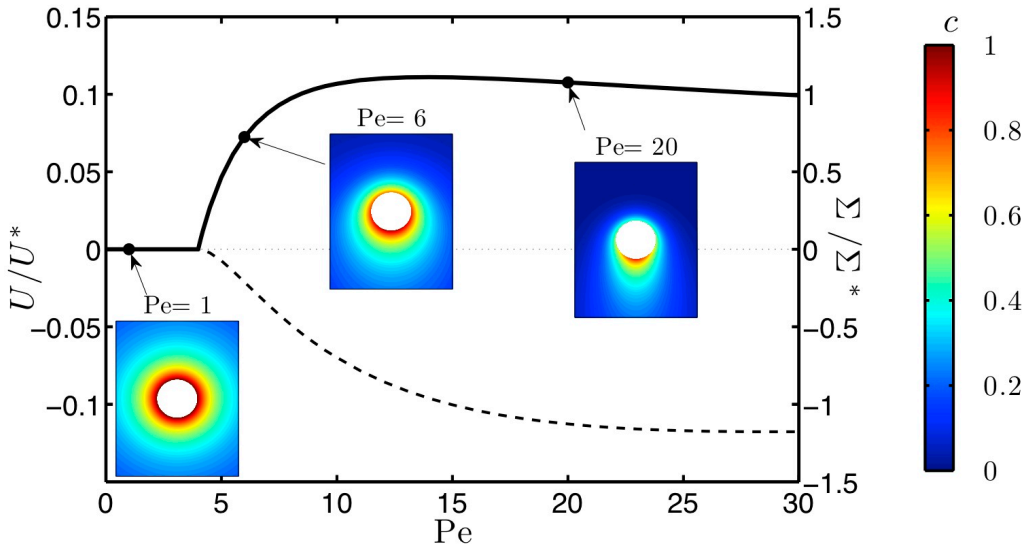

FIG. 1: Evolution with $\mathrm{Pe} = U^* a/D$ of the non-dimensional droplet velocity U/U^* with $U^* = |AM'|/D$ and the non-dimensional stresslet $10\pi\alpha_2^o$. The non-dimensional relative concentration $c = (C - C_\infty)/(Aa/D)$ is also shown for selected Pe, showing the symmetry breaking in the solute distribution associated with self-propulsion, despite the isotropy of the solute flux at the droplet boundary.